Biomimetic nanostructured antireflection coating and its application on crystalline silicon solar cells

J.Y. Chen,[1] W.-L. Chang,[2] C.K. Huang,[1] and K.W. Sun[1,*]

[1] *Department of Applied Chemistry, National Chiao Tung University, Hsinchu, Taiwan*
[2] *Green Energy & Environment Research Laboratories (GEL), Industrial Technology Research Institute (ITRI), Hsinchu, Taiwan*
**kwsun@mail.nctu.edu.tw*

Abstract: In this report, we demonstrate the implementation of biomimetic nanostructured antireflection coatings with polymethyl methacrylate (PMMA) layer on the micro-textured surface of silicon crystalline solar cells. To reduce cost, the process combines colloidal lithography, cast molding method, and reversal nanoimprint lithography. The technique is simple, low cost, and does not cause damage to the thin and brittle conventional crystalline solar cells. The antireflection properties of this biomimetic nanostructure coating are considered as effective as those of a conventional single-layer SiN_x thin film. The resultant structures alone could reduce the average reflectance of solar cell from 13.2% to 7.8% and enhance power conversion efficiency from 12.85% to 14.2%.

OCIS codes: (310.1210) Antireflection; (310.6628) Subwavelength structures, nanostructures; (040.5350) Photovoltaic.

References and links

1. S. Chattopadhyay, Y. F. Huang, Y. J. Jen, A. Ganguly, K. H. Chen, and L. C. Chen, "Anti-reflecting and photonic nanostructures," Mater. Sci. Eng. Rep. **69**(1-3), 1–35 (2010).
2. M. Y. Chiu, C. H. Chang, M. A. Tsai, F. Y. Chang, and P. C. Yu, "Improved optical transmission and current matching of a triple-junction solar cell utilizing sub-wavelength structures," Opt. Express **18**(S3 Suppl 3), A308–A313 (2010).
3. J. Y. Chen and K. W. Sun, "Enhancement of the light conversion efficiency of silicon solar cells by using nanoimprint anti-reflection layer," Sol. Energy Mater. Sol. Cells **94**(3), 629–633 (2010).
4. K. S. Han, J. H. Shin, W. Y. Yoon, and H. Lee, "Enhanced performance of solar cells with anti-reflection layer fabricated by nano-imprint lithography," Sol. Energy Mater. Sol. Cells **95**(1), 288–291 (2011).
5. Y. F. Li, J. H. Zhang, and B. Yang, "Antireflective surfaces based on biomimetic nanopillared arrays," Nano Today **5**(2), 117–127 (2010).
6. Y. F. Huang, S. Chattopadhyay, Y. J. Jen, C. Y. Peng, T. A. Liu, Y. K. Hsu, C. L. Pan, H. C. Lo, C. H. Hsu, Y. H. Chang, C. S. Lee, K. H. Chen, and L. C. Chen, "Improved broadband and quasi-omnidirectional anti-reflection properties with biomimetic silicon nanostructures," Nat. Nanotechnol. **2**(12), 770–774 (2007).
7. J. Q. Xi, M. F. Schubert, J. K. Kim, E. F. Schubert, M. F. Chen, S. Y. Lin, W. Liu, and J. A. Smart, "Optical thin-film materials with low refractive index for broadband elimination of Fresnel reflection," Nat. Photonics **1**, 176–179 (2007).
8. P. C. Yu, C. H. Chang, C. H. Chiu, C. S. Yang, J. C. Yu, H. C. Kuo, S. H. Hsu, and Y. C. Chang, "Efficiency Enhancement of GaAs Photovoltaics Employing Antireflective Indium Tin Oxide Nanocolumns," Adv. Mater. (Deerfield Beach Fla.) **21**(16), 1618–1621 (2009).
9. Y. J. Lee, D. S. Ruby, D. W. Peters, B. B. McKenzie, and J. W. P. Hsu, "ZnO nanostructures as efficient antireflection layers in solar cells," Nano Lett. **8**(5), 1501–1505 (2008).
10. J. Y. Chen and K. W. Sun, "Growth of vertically aligned ZnO nanorod arrays as antireflection layer on silicon solar cells," Sol. Energy Mater. Sol. Cells **94**(5), 930–934 (2010).
11. H. L. Chen, S. Y. Chuang, C. H. Lin, and Y. H. Lin, "Using colloidal lithography to fabricate and optimize sub-wavelength pyramidal and honeycomb structures in solar cells," Opt. Express **15**(22), 14793–14803 (2007).
12. C. H. Sun, P. Jiang, and B. Jiang, "Broadband moth-eye antireflection coatings on silicon," Appl. Phys. Lett. **92**(6), 061112 (2008).
13. Y. F. Li, J. H. Zhang, S. J. Zhu, H. P. Dong, F. Jia, Z. H. Wang, Z. Q. Sun, L. Zhang, Y. Li, H. B. Li, W. Q. Xu, and B. Yang, "Biomimetic Surfaces for High-Performance Optics," Adv. Mater. (Deerfield Beach Fla.) **21**, 4731–4734 (2009).

#147848 - $15.00 USD Received 23 May 2011; revised 26 Jun 2011; accepted 30 Jun 2011; published 12 Jul 2011

14. J. Zhu, Z. F. Yu, G. F. Burkhard, C. M. Hsu, S. T. Connor, Y. Q. Xu, Q. Wang, M. McGehee, S. H. Fan, and Y. Cui, "Optical absorption enhancement in amorphous silicon nanowire and nanocone arrays," Nano Lett. **9**(1), 279–282 (2009).
15. N. C. Linn, C. H. Sun, P. Jiang, and B. Jiang, "Self-assembled biomimetic antireflection coatings," Appl. Phys. Lett. **91**(10), 101108 (2007).
16. C. J. Ting, M. C. Huang, H. Y. Tsai, C. P. Chou, and C. C. Fu, "Low cost fabrication of the large-area anti-reflection films from polymer by nanoimprint/hot-embossing technology," Nanotechnology **19**(20), 205301 (2008).
17. B. Paivanranta, T. Saastamoinen, and M. Kuittinen, "A wide-angle antireflection surface for the visible spectrum," Nanotechnology **20**(37), 375301 (2009).
18. Q. Chen, G. Hubbard, P. A. Shields, C. Liu, D. W. E. Allsopp, W. N. Wang, and S. Abbott, "Broadband moth-eye antireflection coatings fabricated by low-cost nanoimprinting," Appl. Phys. Lett. **94**(26), 263118 (2009).
19. J. Zhu, C. M. Hsu, Z. F. Yu, S. H. Fan, and Y. Cui, "Nanodome solar cells with efficient light management and self-cleaning," Nano Lett. **10**(6), 1979–1984 (2010).
20. J. Rybczynski, U. Ebels, and M. Giersig, "Large-scale, 2D arrays of magnetic nanoparticles," Colloid Surface A **219**(1-3), 1–6 (2003).
21. C. Li, G. S. Hong, P. W. Wang, D. P. Yu, and L. M. Qi, "Wet Chemical Approaches to Patterned Arrays of Well-Aligned ZnO Nanopillars Assisted by Monolayer Colloidal Crystals," Chem. Mater. **21**(5), 891–897 (2009).
22. N. Koo, M. Bender, U. Plachetka, A. Fuchs, T. Wahlbrink, J. Bolten, and H. Kurz, "Improved mold fabrication for the definition of high quality nanopatterns by soft UV-nanoimprint lithography using diluted PDMS material," Microelectron. Eng. **84**(5-8), 904–908 (2007).

1. Introduction

The performance of a solar cell is critically dependent on the absorption of incident photos and their conversion to current. Inasmuch as more than 30% of incident light is reflected from the silicon surface back to the air, an antireflection (AR) layer is a typical type of coating which can be applied to the surface to reduce light reflection and to increase light absorption. In conventional silicon solar cells, silicon nitride (with a refractive index of 2.0) has been used in single-layer thin-film antireflection coating materials. The thin film configuration creates double interfaces and results in two reflected waves. When these two waves are out of phase, destructive interference occurs, cancelling both beams partially or totally before they exit the surface [1]. The destructive interference occurs in normal incident light only at a particular wavelength. It also depends on the reflective index of the coating material. Therefore, the AR effect of a single-layer thin-film coating is rather limited. To get better AR effect, periodic nanostructures with gradient refractive indices become an ideal AR coating in next-generation optoelectronic devices [2–4].

Periodic nanostructures, which are found in insects, like moth and some butterflies, provide inspiration for scientists to define both morphology and dimensions, and produce the desired functionality for many important applications [1, 5]. The biomimetic structures, which have been used for AR purposes, provide valuable clues to gradient refractive index fabrication and design for efficient AR structures. Biomimetic AR structure with surface relief gratings may be understood in terms of a thin film, in which the refractive index changes gradually and continuously from the top of the structure to the bulk materials. The period of the so-called sub-wavelength structures (SWSs) is sufficiently smaller than the wavelength of incident light, so that the structures cannot be resolved by the incident light. The direction of the first diffracted order is over the horizon. The SWS can dramatically suppress the reflection and increase light transmission simultaneously at the interface, over a wide range of angles and wavelengths [6–18], because the surfaces have many tunable factors, such as period, depth, and cross-sectional geometry. In addition to their high-performance optical properties, SWS arrays exhibit self-cleaning capability because of the high fraction of air trapped in the trough area between arrays [19].

Tapered SWS could be fabricated using various techniques which involve lithography and etching. Recently, to avoid high costs or methods unsuitable for making SWSs with large areas, versatile techniques have emerged as promising candidates for fabricating AR nanostructures, such as self-masked dry etching [6], oblique-angle deposition [7,8], nanorods synthesis [9, 10], colloidal lithography [11–14], and nanoimprint lithography [15–18].

#147848 - $15.00 USD Received 23 May 2011; revised 26 Jun 2011; accepted 30 Jun 2011; published 12 Jul 2011

Colloidal lithography is a low-cost and relatively high-throughput method for patterning nanostructures and has been widely used to fabricate biomimetic structures, such as moth eye and honeycomb. Using the interface method, the nanospheres are arranged into a hexagonal close-packing monolayer. The advantages of reversal nanoimprint lithography are its low cost, low imprint pressure, and ability to imprint on rough surfaces, such as the textured surface of solar cells. In this report, we demonstrate the implementation of a biomimetic nanostructure antireflection coating by combining reversal nanoimprint lithography, colloidal lithography, and cast molding method. Our biomimetic AR layer was demonstrated on conventional crystalline solar cells, and the overall AR effects were compared with a typical single-layer SiN_x coating. This combined technique provides a simple, scalable, and cost-effective process to modify AR structures.

2. Experiment process

Figure 1 shows the making processes and the structure illustrations of our nanostructured AR coating on conventional crystalline solar cells. First, we used an interface method developed by Giersig et al. [20, 21], with some modifications, for depositing polystyrene (PS) nanospheres. The mold in Fig. 1(a) is a silicon wafer, with its surface deposited with a 1 um-thick silicon nitride layer using plasma-enhanced chemical vapor deposition (Oxford Instrument, Plasmalab 80 Plus). The surface of the mold and a 2 cm^2 square glass were made hydrophilic by immersing them in piranha solution (H_2SO_4: H_2O_2 = 3:1) at 80°C for 1hr. The square glass was placed inside a glass vessel (middle-bottom part), and then de-ionized (D.I.) water was added slowly to the vessel until the water level was near the lip of the glass but not covering the top of the glass. Two types of PS nanospheres (purchased from Golden Innovation Corp.), with diameters of 250 nm and 500 nm, were diluted in a 10 wt. % water solution by mixing them with an equal amount of ethanol. We dropped 15 µl of the 250 nm nanosphere solution (25 µl for the 500 nm nanosphere solution) on top of the glass, which spread freely to cover the water surface with an unordered monolayer. To further consolidate the spheres to form a closely packed monolayer, the water surface tension was changed by adding a few µl of 5% dodecylsodiumsulfate solution. After this process, a highly ordered nanosphere monolayer covered a large area. The monolayer was then lifted from the water with the previously mentioned Si substrate. A monolayer of closely packed arrays of PS nanospheres was formed on the template surface after drying at 70 °C. The silicon nitride layer on the Si template was then etched using an inductively-coupled plasma-reactive ion etching (ICP-RIE) system (Oxford Instrument, Plasmalab System 100), using the monolayer PS nanosphere arrays as hard mask. The sidewall profile of the nanostructures could be modified with a smooth gradient by controlling the gas flow of CHF_3 and O_2, chamber pressure, and etching time. The etching parameters are listed in Table 1.

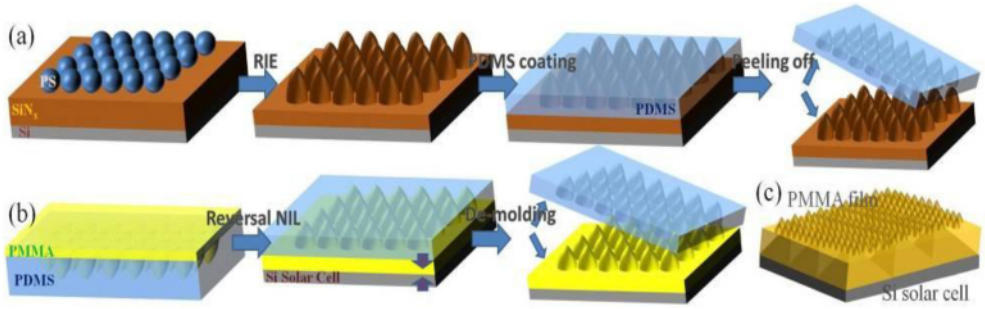

Fig. 1. Schematics and flow chart of the biomimetic nanostructure making processes (a) Si mold fabrication using the colloidal lithography and duplication of the Si mold with PDMS (b) reversal nanoimprint lithography and (c) illustration of surface textured crystalline Si solar cell with nanostructured PMMA AR coating.

#147848 - $15.00 USD Received 23 May 2011; revised 26 Jun 2011; accepted 30 Jun 2011; published 12 Jul 2011

Table 1. ICP-RIE parameters (sizes of PS nanosphere, etching gas flow rate, and etching time) and nanostructure profiles (pitch and depth) of sample structures NS1, NS2, NS3, and NS4.

Parameters / Sample	PS size (nm)	Etching gas flow rate ratio(O_2:CHF_3)(sccm)	Etching time (min)	Period (nm)	Depth (nm)
NS1	500	5:5	10	500	200
NS2	500	10:30	10	500	500
NS3	250	8:40	8	250	200
NS4	250	10:30	6	250	200

To be able to imprint on the thin and brittle conventional crystalline solar cells (with a thickness of only 200 μm), patterns on the Si mold were duplicated onto a soft and flexible polydimethylsiloxane (PDMS, Sylgard 184) mold using a cast-molding process [22]. PDMS is used as standard mold material because of its favorable properties, which include elastomeric character, low price, high optically transparency, low surface energy, and easy molding. If the mold and substrate were both rigid, there is a high probability that they could not make uniform contact. The substrate could also be damaged by unexpected surface protrusions, such as defects and electrodes. It would be difficult to de-mold completely. As such, we used PDMS as a soft and flexible mold to overcome problems encountered when imprint is made using a rigid mold on a non-planar surface with textures and front electrodes.

Nanostructured Si molds were placed in a closed bottle filled with vaporized 1H,1H,2H,2H-perfluoro-octyltrichlorosilane at 250 °C for 1 hr. This mold release agent, which is coated on the surface, can facilitate later the separation of the replicas from Si molds. PDMS, the base material, was first mixed with its curing agent at a ratio of 10:1, and then diluted again by mixing it with toluene at 60% weight concentration to lower its viscosity so that PDMS can completely filled up the Si mold features during the spin-coating process. The material mixtures were spin-coated onto the Si molds at 3000 rpm for 90 s and degassed subsequently. The mold with PDMS coating was immersed in a flat-bottom container filled with a PDMS mixtures to a height of 5 mm. Finally, the container was cured at 60°C for 12 hr.

After de-molding, a layer of polymethyl methacrylate (PMMA), with a 950 K molecular weight and 15% solid contents in anisole, was spin coated on replicated PDMS mold at 3000 rpm, as shows in Fig. 1(b). PMMA has the property of optical transparency, proven weatherability, excellent thermal shock resistance (up to 100 degree Celsius) and is chemically inert to most elements and compounds. It has been widely used as a transparent polymer for various indoor and outdoor applications, such as optics and optic-electronics, signboard, rain shelter, and light dome. The combination of strength, thermal stability, and UV transparency makes it an excellent coating material under outdoor light-exposure conditions. There are also other alternatives with improved UV resistance, such as polycarbonate, cycloaliphatic epoxy, hydrogenated epoxy, and perfluorinated acrylic polymer, which can be used to replace the PMMA. Here, the PMMA layer, with a medium refractive index value (1.49) between silicon (with a refractive index of 3.5) and air, also serves as an adhesive layer to bind the replicated PDMS mold with the Si solar cells during reversal nanoimprint process. There is no need for any release agent between PDMS and PMMA. The thickness of spin-coated PMMA film was almost 3 μm and completely filled up the rough surfaces of solar cells.

In this work, a crystalline Si solar cell was prepared through commercial fabrication processes. The p-type Si wafers were roughened using KOH saw damage etch with no additional texturization. A 200 nm n-type layer was created on the texture by $POCl_3$ diffusion using a centrotherm tube furnace to form a p-n junction, followed by the depositing of a surface passivation layer of 10 nm SiN_x using a centrotherm direct plasma PECVD furnace. Front and rear side fingers and bus bar contacts were screen-printed with a standard, commercially available lead-containing Ag paste, Al paste, and Ag + Al paste using a semi-automatic ATMASC 25PP printer. The cells were fired using a fast-firing conveyor belt furnace at an optimal firing temperature of 850 °C to make the fingers and the bus bars come

#147848 - $15.00 USD Received 23 May 2011; revised 26 Jun 2011; accepted 30 Jun 2011; published 12 Jul 2011

into contact with the n- and the p-type regions for maximum performance. Finally, the cell edges were isolated using a 532 nm Nd:YAG laser cutting tool. The solar cell device and the PDMS mold with the coated PMMA layer were then combined and placed on the sample stage in our home-made nanoimprintor. The PMMA films were hot-embossed at a temperature of 120 °C under a pressure of 0.2 kg/cm^2. The pressure was relieved and the sample was de-molded after the stage cooled to room temperature. As show in Fig. 1(c), the PMMA thin film with nanostructures was imprinted onto the micro-textured surface of a crystalline Si solar cell.

3. Results and Discussion

Figure 2(a) shows the top view SEM image of the 500 nm PS nanosphere monolayer arrays after colloidal lithography. The nanosphere arrays shown in Fig. 2(a) are already slightly etched with oxygen plasma to create space between spheres so that etching gases in a later ICP-RIE process could penetrate underneath the nanospheres more easily. In the RIE process, reactive O_2 gas is used to etch the polystyrene spheres; reactive CHF_3 gas is used to remove the underlying silicon nitride layer. Based on the reactive gases ratio, the periodic nanostructures from the nanosphere arrays are transferred to the substrate and create a profile with a tapered angle cone shape, as show in Fig. 2(b). The nanonipple structures in Fig. 2(b), which we refer to throughout this article as the NS1 structure, have a period of 500 nm and a depth of 250 nm. A SEM image of the replicated PDMS mold from the Si template with the NS1 structures is also given in Fig. 2(c). Finally, the replicated PDMS mold with a coated PMMA layer is reversely imprinted onto a crystalline Si solar cell device, which has pyramidal microtextures on its surface. Figure 2(d) shows a SEM image of imprinted PMMA nanodome arrays, whose shape resembles that of moth eyes.

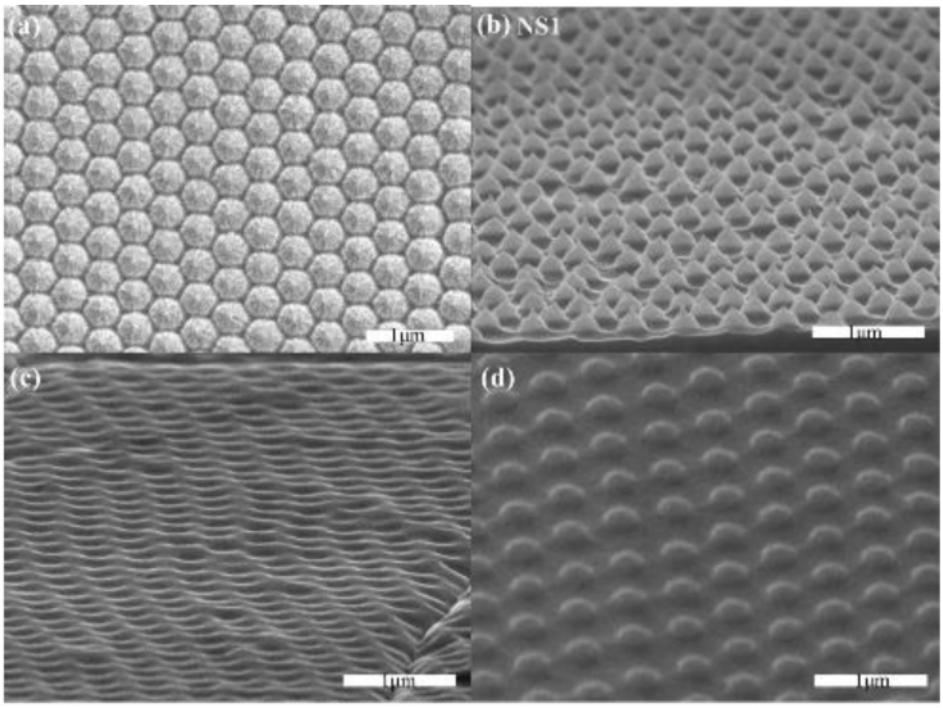

Fig. 2. SEM images of (a) top view of the PS nanosphere arrays (b) Si mold with the NS1 nanostructures (c) the duplicated PDMS mold and (d) the imprinted structures on the PMMA layer.

To investigate geometrical effects on the AR performance of our nanostructured PMMA layers, we fabricated arrays with different periods and surface morphologies using

#147848 - $15.00 USD Received 23 May 2011; revised 26 Jun 2011; accepted 30 Jun 2011; published 12 Jul 2011

nanospheres with different diameters and RIE parameters. Three other Si mold structures, which we refer to as NS2, NS3, and NS4 throughout this article, were also fabricated, with their profiles summarized in Table 1. Figures 3(a) to 3(c) show SEM images of the three Si molds (NS2, NS3, and NS4). Their final imprinted results on PMMA are also given in Figs. 3(d) to 3(f), respectively. The NS2 structure, as shown in Fig. 3(a), has a sharp nanocone shape with a period of 500 nm and a depth of 500 nm. The NS3 structure shown in Fig. 3(b) has a smooth gradient, which resembles moth-eye structures with a period of 250 nm. Its imprinted structure, as shown in Fig. 3(e), forms nanodome arrays with a depth of 200 nm. The inset in Fig. 3(e) shows moth-eye structures with a closely ordered and smooth profile. The NS4 structure, as shown in Fig. 3(c), shows sharp nanocone arrays with a period of 250 nm. The imprinted PMMA structure in Fig. 3(f) has a depth of 200 nm.

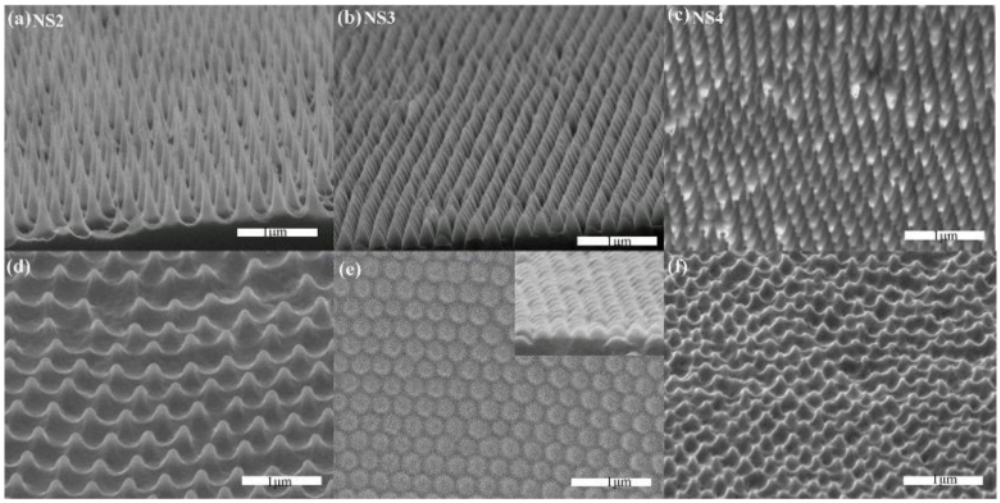

Fig. 3. SEM images of molds with nanostructures of (a) NS2 (b) NS3 and (c) NS4. SEM images of the final imprinted PMMA structures from nanostructure profiles of (a) to (c) are displayed in (d)-(f).

We compared the AR performance of solar cells with the nanostructured PMMA layers (NS1-NS4) only, cells deposited with a conventional 80 nm silicon nitride AR coating only, and devices without any AR coating (bare Si solar cell). The reflectance spectra of the solar cell devices were measured using an UV/Visible/NIR spectrophotometer (Hitachi U-4100), with an integrating sphere for wavelengths ranging from 300 to 1100 nm. Figures 4(a) to 4(d) show the reflectance spectra of samples with different nanostructure profiles. Reflectance spectra of devices with and without silicon nitride AR coating are also displayed in parallel for comparison. Solar cells with a silicon nitride monolayer AR coating only exhibit a typical V-shaped spectrum with a target wavelength at ~500 nm. However, all our four nanostructured PMMA layers give a much flatter response throughout the entire spectrum range. Although the silicon nitride AR coating has a better response in the visible, but it is outperformed by our devices in both the UV and the NIR.

#147848 - $15.00 USD Received 23 May 2011; revised 26 Jun 2011; accepted 30 Jun 2011; published 12 Jul 2011

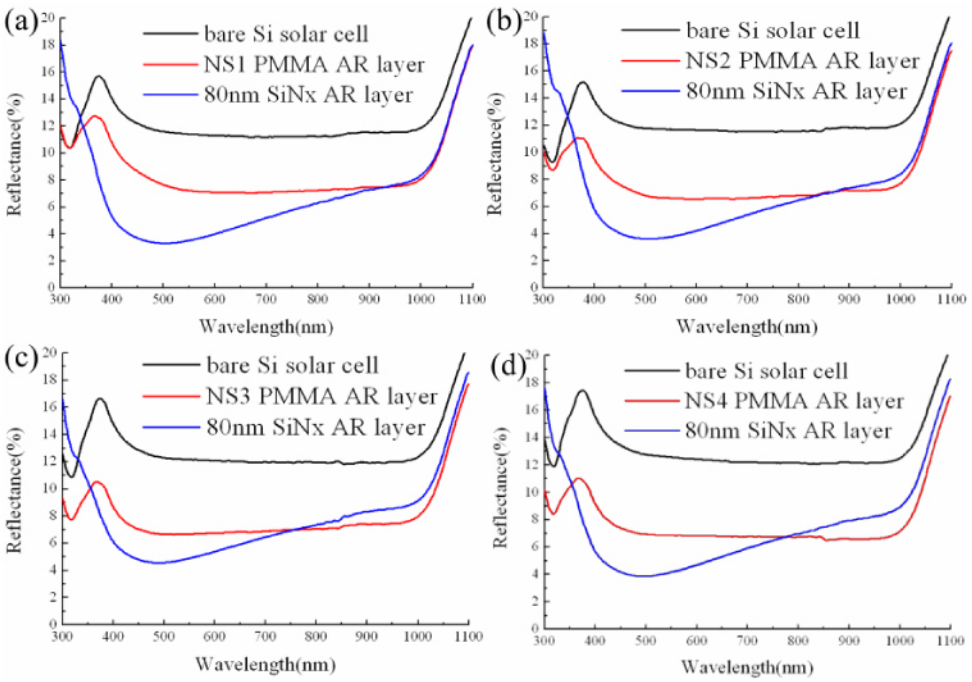

Fig. 4. Reflectance spectra of solar cell devices with the PMMA AR layers of four different nanostructured profiles. Devices without any AR layer and with silicon nitride coating only are also displayed in parallel for comparison.

The PMMA layers imprinted with the NS1 and the NS2 structures have a lower AR effect at the UV range compared with the other two structures, NS3 and NS4, because the periods in these two structures are larger than the wavelengths of the UV light. Hence, nanostructures with a 250 nm period are more suitable for AR applications extended in the UV. The average reflectance (averaged from 300 to 1100 nm) of a surface covered with the NS1 structures dropped by ~28.7% (relative to the bare Si solar cell). On account of a higher aspect ratio, samples with the NS2 structures gave a higher AR effect (relative reflectance dropped by ~35.5%). However, the AR layers with NS3 and NS4 structures had even lower average reflectance of 7.8% and 8%, respectively, which are comparable to the average reflectances of the silicon nitride AR coatings (7.5% and 7.9%, as shown in Figs. 4(c) and 4(d)).

Photocurrent of the solar cells tested was also analyzed using a solar simulator under Air Mass 1.5 Global (AM 1.5G) illumination condition (100 mW/cm^2, 25 °C). Again, we compared I-V characteristics of cells without any AR coating, with nanostructured PMMA layer of the NS3 profile only, and with a silicon nitride AR coating only. The measured current-voltage characteristics are plotted in Fig. 5. Inset in Fig. 5 shows an oblique photograph taken from the devices with nanostructured PMMA layers (on the left) and silicon nitride coatings (on the right). The sharp contrast between the two devices indicates a visible difference in reflectance at conditions other than normal incidence. The I-V curve of the solar cell device with the NS3 nanostructured PMMA coating only almost overlaps with the curve of the device with the silicon nitride AR layer only. The open-circuit voltage and the fill factor remain unaffected, which proves that there were no damages made to the devices during the reversal nanoimprint process.

#147848 - $15.00 USD Received 23 May 2011; revised 26 Jun 2011; accepted 30 Jun 2011; published 12 Jul 2011

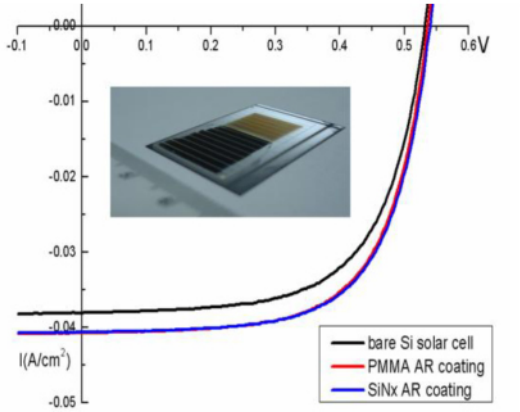

Fig. 5. AM 1.5G I-V characteristics of the Si single crystalline solar cells, without any AR coating, with NS3 nanostructure PMMA AR coating only, and with a 80 nm-thick silicon nitride AR coating only. Inset shows the oblique photograph of device with NS3 nanostructures PMMA only (on the left) and with a 80 nm-thick silicon nitride coating only (on the right).

Table 2 summarizes performance and I-V characteristics of all four samples. The improvement in short-circuit current, accompanied by the enhancement of power conversion efficiency, is attributed to the reduced reflectance with AR coatings. Our best result shows an increase of 1.35% in conversion efficiency (from 12.85% to 14.2%) with just the NS3 structured PMMA AR layer on the solar cells. We believe that, with further improvement in the aspect ratio, the performance of our broadband PMMA AR layers can easily surpass the conventional single silicon nitride AR layer.

Table 2. Current-voltage characteristics of open circuit voltage (V_{oc}), short circuit current (I_{sc}), and power conversion efficiency (PEC) at AM 1.5G and average reflectance between 300 – 1100 nm (R) of solar cells with different AR coatings.

		V_{oc}(V)	I_{sc}(mA/cm^2)	PCE(%	R(%)
Sample 1	Bare	0.540	38.23	13.56	12.2
	NS1	0.544	40.00	14.38	8.7
	SiNx	0.545	40.59	14.68	7
Sample 2	Bare	0.543	38.29	13.30	12.4
	NS2	0.541	40.83	14.27	8
	SiNx	0.545	40.87	14.48	7.2
Sample 3	Bare	0.532	38.05	12.85	13.2
	NS3	0.537	40.68	14.20	7.8
	SiNx	0.540	40.58	14.29	7.5
Sample 4	Bare	0.527	38.30	12.46	12.9
	NS4	0.530	40.30	13.43	8
	SiNx	0.532	40.40	13.49	7.9

4. Conclusion

In summary, we have successfully imprinted a nanostructured PMMA layer onto the micro-textured surface of Si crystalline solar cells without damaging the devices. The processes combining colloidal lithography, cast molding method, and reversal nanoimprint lithography are simple, low cost, and cause no damages on the thin and brittle conventional crystalline solar cells. The resulting biomimetic nanostructures reduce the average reflectance from 13.2% to 7.8% and enhanced power conversion efficiency of solar cells from 12.85% to 14.2%. With their broadband AR response and wide incident angle range, they have the potential to replace conventional single-layer AR coatings for optical and electro-optical device applications.

#147848 - $15.00 USD Received 23 May 2011; revised 26 Jun 2011; accepted 30 Jun 2011; published 12 Jul 2011

Acknowledgments

This work was supported by the National Science Council of the Republic of China under Contract No. NSC 99-2119-M-009-004-MY3.

#147848 - $15.00 USD Received 23 May 2011; revised 26 Jun 2011; accepted 30 Jun 2011; published 12 Jul 2011